Estimation of gravity wave parameters to alleviate the delay in the Antarctic vortex breakup in general circulation models

Guillermo Scheffler[a] and Manuel Pulido[b]*

[a] *Department of Mathematics, FACENA, Universidad Nacional del Nordeste, Corrientes, Argentina*
[b] *Department of Physics, FACENA, Universidad Nacional del Nordeste, and CONICET, Corrientes, Argentina*
*Correspondence to: Department of Physics, FACENA, Universidad Nacional del Nordeste, Av. Libertad 5400, Corrientes (3400), Argentina; pulido@exa.unne.edu.ar

The impact of optimal parameters in a non-orographic gravity wave drag parameterization on the middle atmosphere circulation of the Southern hemisphere is examined. Optimal parameters are estimated using a data assimilation technique. The proposed technique aims to reduce the delay in the winter vortex breakdown of the Southern Hemisphere found in general circulation models, which may be associated with a poor representation of gravity wave activity. We introduce two different implementations of the parameter estimation method: an *offline* estimation method and a *sequential* estimation method. The delay in the zonal-mean zonal-wind transition is largely alleviated by the optimal gravity wave parameters. The sequential method diminishes the model biases during winter vortex evolution, through gravity wave drag alone. On the other hand, the offline method accounts better for the unresolved-resolved wave interactions and the zonal-wind transition. We show that the final warmings in the lower mesosphere are mainly driven by planetary wave breaking. These are affected by changes in the gravity wave drag which are responsible for the stratospheric preconditioning. Parameter estimation during the vortex breakdown is a challenging task that requires the use of sophisticated estimation techniques, because there are strong interactions between unresolved gravity wave drag and planetary waves. Copyright © 0000 Royal Meteorological Society

Key Words: gravity wave parameterizations, parameter estimation, model bias, final stratospheric warming

Received . . .

Citation: . . .

1. Introduction

The physical processes that drive the climate encompass a large range of temporal and spatial scales that cannot be included in the numerical equations of a general circulation model. The unresolved processes are represented through physical parameterizations which establish functional dependences with the resolved variables through a set of unknown parameters. The inference of parameter values aims to improve the agreement between model integrations and observations, even if the role of the parameter is not completely understood within the model (Randall et all. 1997). This inference can be achieved by either manual tuning, through trial-and-error sensitivity experiments, or with more sophisticated techniques involving sequential data assimilation. Sequential data assimilation methods can be readily reformulated to conduct a joint state-parameter estimation (Anderson 2001). The ensemble Kalman filter has been successfully applied to estimate parameters from earth system models (Annan et al. 2005). An extensive review of ensemble-based data assimilation techniques for parameter estimation is given in Ruiz et al. (2013).

One of the unresolved processes that is parameterized in general circulation models is the propagation and breaking of small-scale gravity waves. The representation of these sub-grid processes through physical parameterizations is critical in models that include the middle atmosphere,

This article has been accepted for publication and undergone full peer review but has not been through the copyediting, typesetting, pagination and proofreading process, which may lead to differences between this version and the Version of Record. Please cite this article as doi: 10.1002/qj.3074

since small-scale gravity waves carry a significant amount of momentum flux vertically from the troposphere to the stratosphere and mesosphere. In this region, they produce a large-scale forcing through their breaking. This forcing produced by unresolved gravity waves is referred to as *missing gravity wave drag*. Parameterizations represent the large-scale effects of gravity wave breaking taking into account the mean flow distribution to determine which gravity waves can reach the stratosphere and mesosphere (Lindzen 1981). Typically, gravity wave drag parameterizations involve the vertical propagation of a wave spectrum which is filtered and saturated according to a criterion (Warner and McIntyre 1996, Hines 1997, and Scinocca 2003).

In the middle atmosphere, the forcing through gravity waves plays a dominant role in driving the equator-to-pole residual circulation (Alexander and Rosenlof 1996) and also in the seasonal cycle of polar temperatures (Alexander et al. 2010), which is critical for long-term modeling of ozone recovery. Furthermore, gravity waves also play an important role in driving the quasi-biennial oscillation. Bushell et al. (2010) showed that over the Equatorial region, parameterized gravity waves may have a significant role in the acceleration of zonal winds. Thus, more realistic mean periods of the quasi-biennial oscillation may be obtained by properly tuning the gravity wave drag parameterization.

The representation of the vortex breakdown, and particularly, the transition from westerlies to easterlies at high latitudes (referred to as final warming from now on) exhibits a delay with respect to the observed transition in most of the current general circulation models (Austin et al. 2003, Eyring et al. 2006, Hardiman et al. 2011). This issue appears to be related to an identified cold-pole bias in the wintertime stratospheric polar vortex in general circulation models which results in a late breakdown of the polar vortex (McLandress et al. 2012). Long et al. (2014) showed that polar temperature biases in free model integrations of the Met Office Unified Model could be partially alleviated by tuning the energy-scale parameter in the non-orographic gravity wave drag parameterization.

Models and reanalysis present two distinct behaviors of final stratospheric warmings. In the Southern hemisphere, the wind transition starts at the mesosphere and then it descends to the stratosphere. While in the Northern hemisphere, the wind transition occurs first in the stratosphere and then in the mesosphere. This has been associated with the most active role of planetary waves during the transition in the Northern hemisphere (Hardiman et al. 2011).

There is some evidence that the drag of unresolved gravity waves and planetary waves have strong interactions in general circulation models (McLandress and McFarlane 1993, McLandress et al. 2012 and Cohen et al. 2013). These interactions seem to work in both directions. Scheffler and Pulido (2015) showed that reducing the non-orographic gravity wave drag triggered a response in the planetary wave drag in the middle atmosphere of the Southern hemisphere that can reduce the biases of the final warming in models. These interaction processes pose a challenge for tuning gravity wave drag parameterizations. Changes in the parameterization produce changes in the general circulation, and these in turn produce changes in the planetary wave propagation which also affect the general circulation in longer-time scales. In this scenario of strong interactions, manual tuning of gravity wave parameters through trial-and-error sensitivity experiments may not be suitable. In the case of objective parameter estimation techniques, they need to capture the time scales of the interactions to give optimal parameters that account for the resolved-unresolved interaction processes.

Pulido and Thuburn (2005, 2006) developed a data assimilation technique that combines a middle atmosphere dynamical model with analysis data to estimate the missing forcing in the middle atmosphere. The technique is based on the four-dimensional variational data assimilation (4d-Var) principles. Pulido and Thuburn (2006) associated the systematic bias between the model and the observations estimated by the data assimilation technique with the missing gravity wave drag from unresolved waves. This variational data assimilation technique was used in Pulido and Thuburn (2008) to estimate the seasonal cycle of missing drag from Met Office analyses. The estimated middle atmosphere missing gravity wave drag at $60°\mathrm{S}$ by Pulido and Thuburn (2008) shows the presence of a seasonal cycle, characterized by a change of sign of the zonal component of missing gravity wave drag between two and five weeks before the zonal wind reversal. The resulting time-mean winter missing drag fields from data assimilation were used in Pulido et al. (2012) to optimize a set of constant parameters in the gravity wave drag parameterization. However, they do not evaluate their impact on model simulations.

In this work, we estimate time-dependent parameters using the data assimilation technique introduced in Pulido et al. (2012) and examine the impact of optimal parameters on model integrations during the stratospheric final warmings in the Southern hemisphere. Furthermore, we evaluate whether the data assimilation technique is able to account for the ubiquitous interactions between unresolved waves represented through parameterizations and resolved large-scale waves. This work is organized as follows, Section 2 describes the NASA's Modern-Era Retrospective Analysis for Research and Applications (MERRA) data (Rienecker et al. 2011) and the model which are used in our experiments. In this section, we also introduce two approaches for estimation of free parameters in the gravity wave drag parameterization: an offline (Section 2.3) and a sequential method (Section 2.4). The results of the missing drag estimation during stratospheric final warmings are described in Section 3.1. They assess the amount of unresolved gravity wave drag that needs to be represented by the parameterization. Results from the parameter estimation with the offline and sequential methods are described in Sections 3.2 and 3.3, respectively. The impact of the optimal parameters in free model integrations on the planetary wave activity is discussed. Finally some conclusions are drawn in Section 4.

2. Methodology

2.1. Data and model details

The data used in this work are the MERRA reanalysis (Rienecker et al. 2011). They are based on the Goddard Earth Observing System Data Assimilation System Version 5 (GEOS-5), which combines the state from an atmospheric general circulation model with observations from multiple sources using a three-dimensional variational data assimilation technique. The analysis step in the data assimilation system is represented by an incremental analysis update

step (Bloom et al. 1996), that leads to a smooth evolution between assimilation windows. The analyses from this assimilation technique are ideal for momentum budget studies since the incremental analysis update avoids the spin-ups produced by the instantaneous inception of momentum.

The numerical model used in this work is the University of Reading middle atmosphere dynamical model. The model solves the full potential vorticity-based hydrostatic dynamical equations in a hexagonal-icosahedral horizontal grid (Thuburn 1997) with a resolution of about 4.5 degrees. The model covers from about $100\,\mathrm{hPa}$ to $0.018\,\mathrm{hPa}$ with 16 isentropic vertical levels. Further details of the model can be found in Pulido and Thuburn (2005). Bottom boundary conditions are imposed with the Montgomery potential at around $100\,\mathrm{hPa}$. The bottom boundary forcing is taken every 6 hours from MERRA reanalysis. This removes an incorrect representation of the generation of tropospheric large-scale disturbances as a possible source of model bias.

The non-orographic gravity wave drag parameterization implemented in the model is the one introduced in Scinocca (2003). The parameterization has been successfully implemented in models such as the CCCMa (Scinocca et al. 2008) and the ECMWF model (Orr et al. 2010). This is a hydrostatic non-rotational spectral gravity wave drag parameterization based on the Warner and McIntyre (1996) framework.

The parameterization represents a time independent and horizontally uniform gravity wave spectrum that is launched in the lower stratosphere and propagates upwards, undergoing processes of back-reflection and critical-level filtering. Because of these processes, the fixed launched gravity wave spectrum produces different gravity wave drag profiles according to the mean wind and temperature profiles in the middle atmosphere, leading to seasonal and latitudinal variations of the gravity wave drag.

The experiments are conducted for the period 2003-2009 (7 years). For each year, the model is started from initial conditions taken from MERRA on January 1st, and integrated during 400 days. With these integrations, we expect to capture the entire cycle of the Southern Hemisphere winter polar vortex. Each year has an independent integration in order to isolate stratospheric final warming biases from each year.

2.2. *Missing forcing estimation*

The missing forcing of the model is estimated using ASDE (Assimilation System for Drag Estimation), a 4d-Var data assimilation system thoroughly described and evaluated in Pulido and Thuburn (2005, 2006). It is based on a conjugate gradients optimization technique. A full adjoint dynamical model is used to evaluate the gradient of the cost function. The control space, i.e. the fields to be estimated, is formed by zonal and meridional drag terms that appear as forcing fields in the right-hand side terms of the model momentum equations.

In this work, MERRA reanalyses are used as observations in the assimilation system. The cost function is composed of the differences between the 'observed' and the model potential vorticity (see Pulido 2014) and differences between observed and model pseudo density (observed pseudo density is derived from 'observed' temperature) between the bottom of the model up to $0.1\,\mathrm{hPa}$.

The estimated missing forcing can be interpreted as the momentum forcing needed by the model to give the closest evolution to the observations (MERRA reanalyses). During the estimation, the model gravity wave drag parameterization is switched off in order to infer the forcing associated with gravity waves and feedback processes with the mean flow.

At every assimilation time window, the model incorporates the estimated missing forcing, giving a forced model evolution that is smooth and very close to the MERRA reanalysis (assuming convergence in the optimization process). The changes in the mean-flow introduced by the incorporation of this missing forcing are expected to produce compensative responses in the breaking of planetary waves as described in Cohen et al. (2014) and Scheffler and Pulido (2015).

The evolution of ASDE is similar to the incremental analysis update (technique used by MERRA) since the model is driven towards the observations through forcing terms. However, ASDE only uses forcing terms in the momentum equations.

2.3. *Offline parameter estimation*

The offline optimization aims to find a set of parameters for the parameterization that leads to a gravity wave drag profile that holds the best resemblance with the missing drag estimated with ASDE. Since the gravity wave drag parameterization is a column-based scheme, where each grid point requires the propagation and filtering of an independent spectrum, a set of parameters can be estimated for each horizontal grid. To reduce the number of free parameters, we assume zonal symmetry —the waves in the parameterization propagate upon zonally averaged winds— so that the control space for each latitude θ_i is defined as $X(\theta_i) = (E^*(\theta_i), \lambda^*(\theta_i), S^*(\theta_i))$ where E^* represents the amount of gravity wave momentum flux launched at the bottom of the model, λ^* the characteristic wavelength of the launched spectrum and S^* a dimensionless saturation parameter.

The parameter optimization is conducted through a genetic algorithm (Goldberg and Holland 1988; Pulido et al. 2012). The algorithm implemented is based on Charbonneau (2002). It is configured with an initial population of 128 individuals and evolved through 150 generations. This algorithm seems suitable since the optimization problem is low dimensional (3 dimensions) in each latitude. On the other hand, the parameterization is highly non-linear and the parameters need to be constrained within reasonable bounds so that the genetic algorithm overcomes the issues of gradient-based optimization Pulido et al. (2012). In this work, E^* was constrained to the range 0.1-5 which proved to be an adequate bound given the sensitivity of the parameter. The other two parameters are constrained to the range 0.1-50 to allow a larger variation of the parameters.

Under these settings, a set of optimal parameters is estimated for each day considering the daily variability of gravity wave drag given by ASDE. This variability has a critical role when modeling the final stratospheric warming (de la Cámara et al. 2016). The parameter estimation is conducted with an offline version of the parameterization, i.e. without the dynamical model. This reduces the computational cost of the parameter optimization technique and allows straightforward computational parallelization.

2.4. *Sequential parameter estimation*

We introduce a second parameter estimation method which will be referred to as *sequential method*. In this method, the parameter estimation procedure is applied sequentially in each assimilation window. First, we estimate the missing gravity wave drag with ASDE, then the optimal parameters are estimated for that assimilation window using the genetic algorithm. Finally, the analysed state is obtained by integrating the model from the previous analysed state using the optimal parameters in the gravity wave drag parameterization. This analysed state is used as an initial condition to estimate the missing gravity wave drag with ASDE in the next assimilation window.

In contrast to the offline method, this approach only accounts for model errors that can be diminished through optimal gravity wave parameters. Other sources of model error are not considered in this method. Possible errors in Rossby wave propagation and breaking due to an incorrect mean flow will not be corrected and eventually at some time they may be solved through gravity wave forcing. Furthermore, the estimated model state in this method is only representing the effects of gravity wave drag given by the parameterization, so that the model biases that are not captured by the parameterization with optimal parameters will give a cumulative effect. Therefore one can foresee the two methods as extreme cases. The offline method computes gravity wave drag for temperature and wind profiles that are the observed ones (or very close to them); while the sequential method computes the gravity wave drag for temperature and wind profiles that represent a free model integration with optimal parameters. The contrasts between the two methods are expected to shed some light on the role of the parameters in the presence of strong resolved-unresolved wave interactions.

The sequential parameter estimation method is computationally more expensive than the offline parameter estimation described in Section 2.3, because the parameter estimation needs to be computed sequentially after the forcing estimation step. Since it is a sequential estimation method, it is not as readily suitable for computational parallelization as the offline method. The parameter optimization and the model integration with the optimal parameters during an assimilation window (1 day) are required before estimating the parameters in the next assimilation window.

3. Results

3.1. *Missing forcing estimation*

Figure 1a shows a 7-year average (2003-2009) of the zonal-mean zonal wind from MERRA averaged between $50°\mathrm{S}$ and $80°\mathrm{S}$. At these latitudes, the wind reversal occurs around mid October in the lower mesosphere (between $1\,\mathrm{hPa}$ and $0.1\,\mathrm{hPa}$), and descends as a slow paced event. The wind reversal at $10\,\mathrm{hPa}$ takes place on average at day 322 (November 18th), shown with a solid vertical line in Fig. 1a.

Figure 1b shows the missing forcing estimated by ASDE using MERRA reanalysis data as observations. During winter, a westward estimated drag in the lower mesosphere is required to decelerate the jet, with peaks of up to $-35\,\mathrm{m\,s^{-1}\,day^{-1}}$ near the top of the model on day 235. The winter stratosphere is characterized by eastward missing forcing, much weaker in comparison to the upper levels, which eventually turns into westward drag to partially drive the zonal wind reversal during spring.

During spring, the vertical structure of the missing forcing is more complex. The dipolar structure is interrupted by an eastward acceleration centre that starts, on average, on day 257 (September 15th), with standard deviation of 13.2 days in the transition date, and has a peak of $16\,\mathrm{m\,s^{-1}\,day^{-1}}$ at $0.4\,\mathrm{hPa}$ on day 279. The drag reversal in the higher stratosphere (between $25\,\mathrm{hPa}$ and $2\,\mathrm{hPa}$) occurs in the mean on day 269, with a standard deviation of 7.1 days. This is 53 days before the wind transition in the mean at $10\,\mathrm{hPa}$.

Figure 2 shows the estimated zonal-mean missing forcing associated with gravity waves as a function of latitude at different stages of the vortex breakdown. The latitudinal variations of the missing forcing are larger during winter (Fig. 2a), when the winter jet reaches its peak. In high latitudes, the vertical structure is dominated by a vertical dipole with a large deceleration centre in the lower mesosphere. This centre is split into two parts. The first one covers from $45°\mathrm{S}$ up the polar region, with a peak of $-30.3\,\mathrm{m\,s^{-1}\,day^{-1}}$ at $62°\mathrm{S}$ and $0.7\,\mathrm{hPa}$ and around $10°$ poleward from the winter jet peak. The second one is in the uppermost part of the deceleration centre and is distributed around mid latitudes, with a peak of $-47\,\mathrm{m\,s^{-1}\,day^{-1}}$ at $54°\mathrm{S}$ around $0.1\,\mathrm{hPa}$. It should be noticed that at these altitudes, the dynamical processes may be affected by the sponge layer at the model top levels ($0.12 - 0.018\,\mathrm{hPa}$). Therefore, we avoid giving a dynamical interpretation to the estimated forcing at these altitudes since it may also be affected by the sponge layer. The large variations in the latitudinal and vertical distribution of missing forcing in the stratosphere stresses the need for latitudinal variations in the parameters associated with sources and filtering in a gravity wave scheme. Source variability in gravity wave parameterizations has been introduced, either by random intermittency (e.g. Lott and Guez 2013; de la Cámara et al. 2016) or by parameterization of convective processes in the troposphere (e.g. Bushell et al. 2015).

During early spring, the vertical structure of the missing forcing is modified by the generation of an eastward forcing above $1\,\mathrm{hPa}$, with a peak of $26\,\mathrm{m\,s^{-1}\,day^{-1}}$ around $45°\mathrm{S}$ (Fig. 2b). During October and November (Fig. 2c), the mid latitudes eastward drag centre is elongated poleward, while the high latitudes westward centre is displaced downward and equatorwards, reaching a maximum of $13\,\mathrm{m\,s^{-1}\,day^{-1}}$ around $45°\mathrm{S}$. The westward forcing in the stratosphere and lower mesosphere continues to decelerate the winter jet, as it descends during spring. The forcing at latitudes polewards of $50°\mathrm{S}$ remains smaller than $15\,\mathrm{m\,s^{-1}\,day^{-1}}$. This is consistent with the weakening and reversal of the zonal wind prior to summer. This vertical structure remains until the subsequent autumn.

During spring, at high latitudes, the estimated missing forcing above $1\,\mathrm{hPa}$ accelerates the zonal mean zonal wind (eastward), even two weeks prior to the final warming. This suggests that the zonal wind reversal at those heights does not depend directly on the gravity wave drag, but on the breaking of planetary waves induced by them (McLandress et al. 2012; Scheffler and Pulido 2015). In Fig. 3a we show the Eliassen-Palm flux divergence derived from the integration that incorporates the missing drag estimated using MERRA reanalysis. During the spring

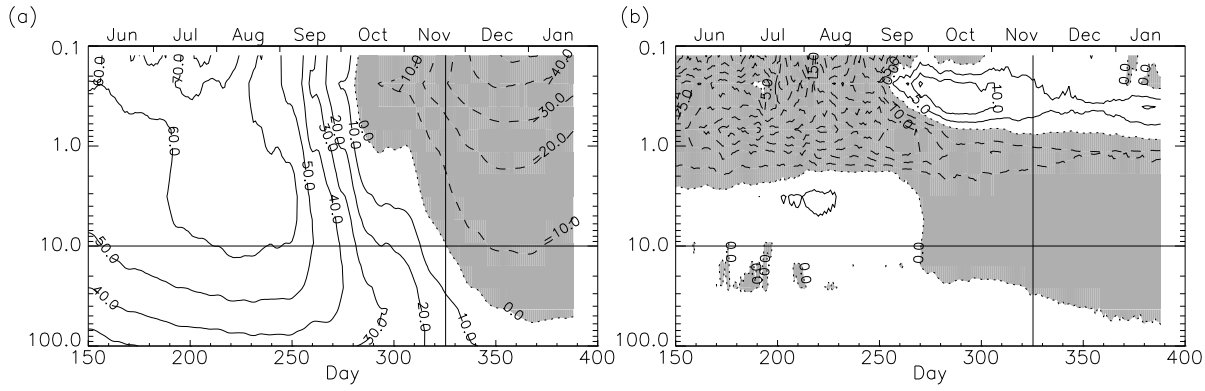

Figure 1. (a) Zonal mean zonal wind averaged between $50°\mathrm{S}$ and $80°\mathrm{S}$ during 2003-2009 as a function of time from MERRA reanalysis (Contour interval is $10\,\mathrm{m\,s^{-1}}$). (b) Zonal mean zonal missing forcing estimated with ASDE. Contour interval is $5\,\mathrm{m\,s^{-1}\,day^{-1}}$. Negative values are shaded. Contours use data smoothed with a 5-day moving average.

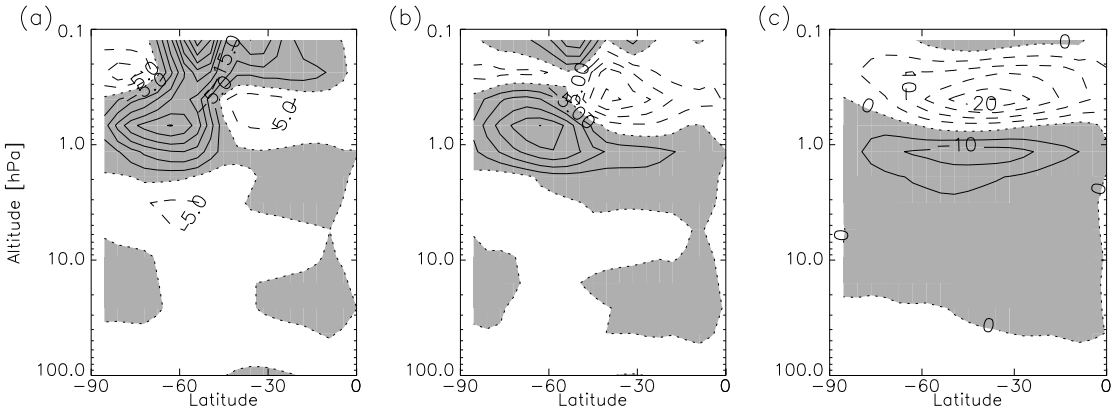

Figure 2. Zonal mean of zonal missing forcing estimated by ASDE as a function of latitude during (a) July-August, (b) September, (c) October and November. Contours at $5\,\mathrm{m\,s^{-1}\,day^{-1}}$.

transition, there is a deceleration (westward forcing) centre in the high stratosphere and lower mesosphere with peaks of $-12.3\,\mathrm{m\,s^{-1}\,day^{-1}}$ on day 266 (September 23th) at $0.4\,\mathrm{hPa}$ and $-11.1\,\mathrm{m\,s^{-1}\,day^{-1}}$ on day 283 (October 10th) at $0.7\,\mathrm{hPa}$. These peaks play an active role in the deceleration of the winter jet. However, the strong deceleration peaks are a consequence of feedback processes between resolved and unresolved forcings. In this sense, the transition to eastward missing drag above $1\,\mathrm{hPa}$ around day 270 occurs shortly after the aforementioned Eliassen-Palm flux divergence peaks.

There are no significant differences between the Eliassen-Palm flux divergence derived from MERRA and from the integration with ASDE (Fig. 3b). This shows the ability of the assimilation technique to drive the model towards reanalyses and so to reproduce accurately the planetary-scale wave drag despite the large daily variability in Eliassen-Palm flux divergence. The model ability to reproduce the MERRA representation of planetary wave drag will be assessed in free model integrations.

3.2. Offline parameter estimation experiments

The optimal parameters were estimated for each day and each latitude using the offline parameter estimation technique. These parameters attempt to reproduce, through the parameterization, the missing forcing estimated by ASDE. Figure 4 shows the estimated values for these parameters, normalized with respect to their standard values (see Subsection 2.3) and averaged at high latitudes of the Southern Hemisphere ($50°\mathrm{S}$ to $80°\mathrm{S}$). Large daily variations were found for each parameter, consistently with ASDE forcing variability so that a 10-day moving average was applied. The launched momentum flux E^* has an evident seasonality, with smaller values during summer and larger values during winter. The maximal values of the E^* parameter are reached during August, when both the zonal wind and the missing drag from ASDE reach their intensity peaks. The period when E^* shrinks coincides with the vortex breakdown. After day 295, E^* becomes lower than 1, suggesting that the drag from the parameterization should be weaker than its standard values.

The parameters λ^* and S^* show low sensitivity leading to an increased daily variability and are, to some extent, correlated. Both show persistent maxima and minima around the same time (see bold lines in Fig. 4b). Parameter λ^* has a consistent global minimum during March, and slowly increases up to its maximum on November. During summer, autumn and early winter (from 0-200 days) S^* is anti-correlated to λ^*. This is a robust behaviour that was present in every year of the 2003-2009 period (not shown). The increase of the value of both parameters coincides with the change of sign of gravity wave drag in the region

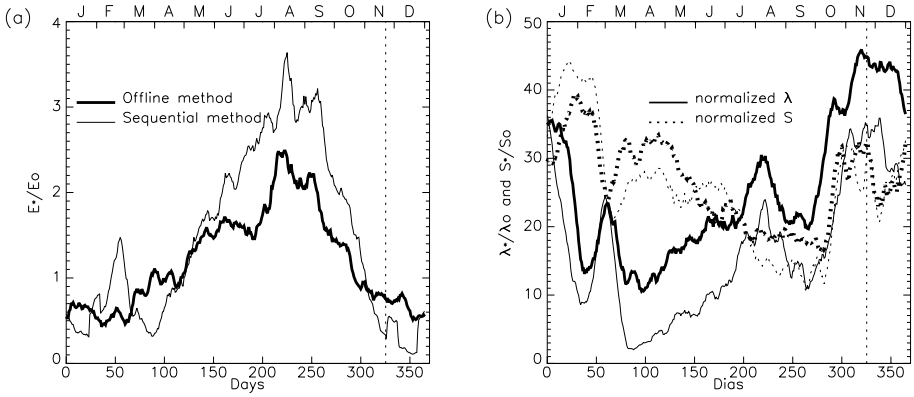

Figure 4. Estimated parameters normalized with respect to their reference values, averaged between $50°\mathrm{S}$ and $80°\mathrm{S}$. Bold lines correspond to the offline method, thin lines correspond to the sequential method for (a) E^* parameter and (b) λ^* (continuous line) and S^* (dotted line). Parameters were smoothed with a 10-day moving average. The vertical dotted line represents the transition day. Reference value for normalization: $E_0 = 10 \times 2.5\sqrt{2}\,10^{-4}\mathrm{Pa}$, $\lambda_0 = 2000\ \mathrm{m}$, and $S_0 = 1$.

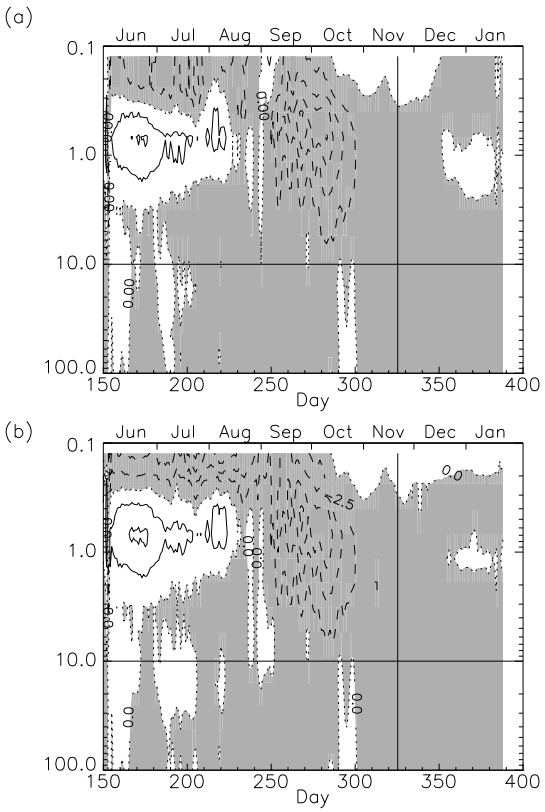

Figure 3. Eliassen-Palm flux divergence averaged between $50°\mathrm{S}$ and $80°\mathrm{S}$ as a function of time derived from (a) the integration with ASDE and (b) MERRA reanalysis. Contours at $2.5\,\mathrm{m\,s^{-1}\,day^{-1}}$. Data were smoothed with a 7-days average window due to the large daily variations.

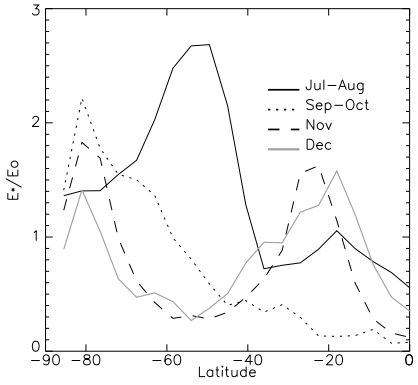

Figure 5. Normalized E^* parameter estimated with the offline method, averaged between days 182 and 243 (i.e. July and August continuous line), between days 260 and 300 (September and October, dotted line), between days 303 and 334 (November, dashed line) and days 335 and 365 (December, grey-continuous line).

between 20-3 hPa (around day 270). Despite the strong correlation and anti-correlation between λ^* and S^*, both parameters need to be estimated. We found in preliminary experiments that excluding either of these two parameters of the estimation leads to suboptimal parameterized forcing and degrades the model state evolution with respect to MERRA (not shown).

The E^* parameter has a strong latitudinal variation that depends on the stage of the vortex breakdown, shown in Fig. 5. During winter, E^* peaks between $45°\mathrm{S}$ and $60°\mathrm{S}$, in accordance with the stratospheric winter jet location. During September and October, the peak is displaced to high latitudes and E^* decreases towards the Equator. This is related to the winter jet annual cycle, since on average, it reaches its largest intensity at $80°\mathrm{S}$ after September 15th. Latitudes equatorwards of $60°\mathrm{S}$ require a launch momentum flux lower than the one provided by the standard value of E^*. During November and December, the launched gravity wave momentum flux is minimal in high latitudes, with the peak of polar regions slowly decaying. This latitudinal pattern persists up to autumn. The E^* parameter shows a peak between $20°\mathrm{S}$ and $25°\mathrm{S}$ that is likely related to the summer jet. The parameter variability in the tropics will not be further analysed since this work focuses on the winter jet and the final stratospheric warming processes. However, these results stress the importance of a temporal and latitudinal dependence of sources in a parameterization of gravity wave drag.

The optimal parameters were incorporated in the model parameterization and the model was integrated

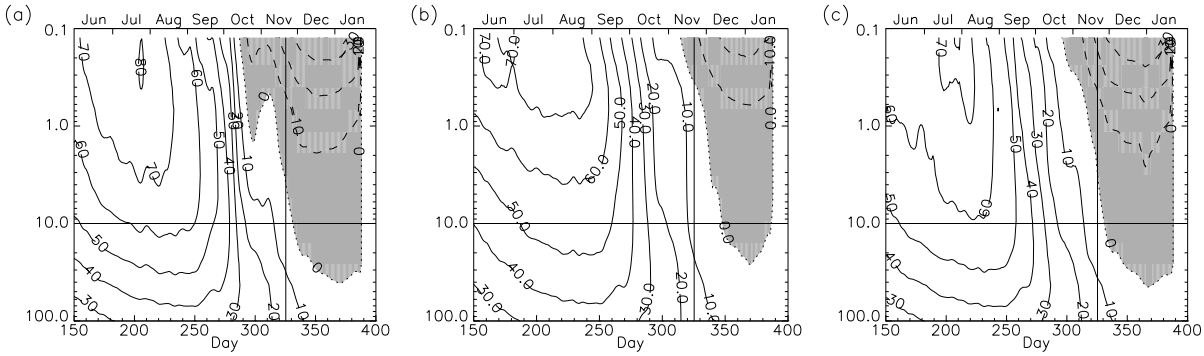

Figure 6. Zonal mean zonal wind averaged between $50°\mathrm{S}$ and $80°\mathrm{S}$ as a function of time for (a) the offline integration, (b) the control integration and (c) the sequential integration. Contour interval is $10\,\mathrm{m\,s^{-1}}$. Negative values are shaded.

using the daily varying zonally symmetric parameters during the seven years starting from initial conditions taken from MERRA every January 1st. The integration using parameters estimated with the offline method will be referred to as *offline integration*. To evaluate the impact of the optimal parameters, we also conducted similar integrations using the standard set of parameters, which we refer to as *control integration*.

Figure 6a shows the zonal-mean zonal wind from the offline integration. The wind reversal near the top of the model occurs on day 286 (October 13th) and progresses downwards slowly as in MERRA, with the wind reversal at $10\,\mathrm{hPa}$ occurring on day 328 (6 days later than in MERRA). This is a large improvement with respect to the control integration (Fig. 6b) where the transition at the top of the model starts in early November and rapidly descends through the stratosphere, with the reversal at $10\,\mathrm{hPa}$ happening around day 339 (December 5th) — excluding years 2007 and 2008 when no wind reversals at $10\,\mathrm{hPa}$ occur. The wind shear for the integration with optimal parameters is more accurate below $10\,\mathrm{hPa}$, but it degrades with altitude, overestimating the jet intensity above $10\,\mathrm{hPa}$. The subsequent summer jet is also intensified by 50% and it is closer to MERRA reanalysis (see Fig. 1a).

The impact of optimal parameters on model integrations is shown in Fig. 7, using the root-mean-squared error (RMSE) integrated vertically from the bottom to $0.4\,\mathrm{hPa}$. The parameter optimization reduces the model error in the zonal-mean zonal wind and temperature consistently up to July compared to the control integration. During July and August, the optimal parameters degrade the circulation and intensify the cold biases. The reason for the poor performance of the offline integration in these months is not clear. This is further discussed in Section 4. During September and October, the impact of optimal parameters on the RMSE is low, but they give a slightly smaller zonal wind and temperature RMSE. During the zonal wind transition a very large impact of optimal parameters is found diminishing significantly the zonal wind and temperature RMSE with respect to the control integration.

Figure 8a shows the gravity wave drag as a function of height and time given by the parameterization in the offline integration. It holds the main vertical features of the missing drag estimated with ASDE (Fig. 1b). The change of sign of gravity wave drag during winter occurs above $5\,\mathrm{hPa}$, unlike the control integration in which it occurs at $20\,\mathrm{hPa}$ (Fig. 8b). The deceleration centre has the characteristic dipolar structure, with a minimum of $-27.7\,\mathrm{m\,s^{-1}\,day^{-1}}$

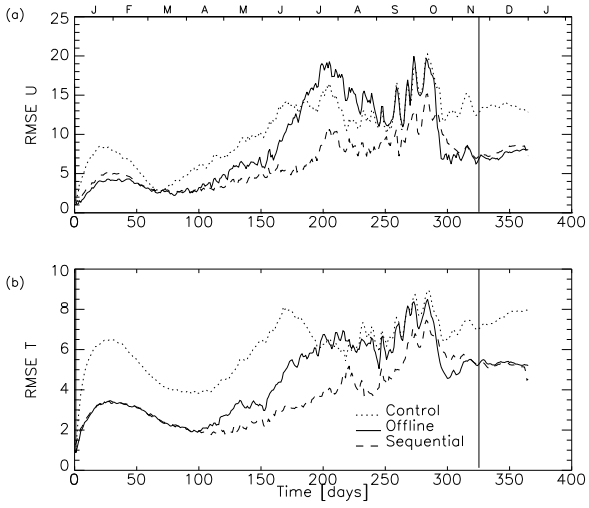

Figure 7. Mean squared error (RMSE) with respect to MERRA, averaged over the latitudinal band $50°\mathrm{S} - 80°\mathrm{S}$ and integrated up to $0.4\,\mathrm{hPa}$ as a function of time for (a) zonal wind and (b) temperature, with the control integration (dotted line), the offline integration (continuous line), and from the sequential integration (dashed line).

at $0.1\,\mathrm{hPa}$. The dipolar structure constitutes a constraint due to momentum flux conservation (Shepherd and Shaw 2004) in the parameterization. In the stratosphere, both the offline and the control integrations give eastward forcing. However, the vertical change from westward to eastward forcing during winter is found at $16\,\mathrm{hPa}$ in the control integration (Fig. 8b) while it is at $2\,\mathrm{hPa}$ in the offline integration. The latter is closer to the vertical structure of ASDE missing forcing. The westward gravity wave drag in the upper stratosphere and lower mesosphere is weaker than in the control experiments between days 260-285, and onwards too. A similar behaviour is found in the missing forcing estimated by ASDE (Fig. 1b). Thus, the anticipation of wind reversal seen in Fig. 6a is not directly associated with gravity wave drag, but instead, to an intensification of Eliassen-Palm flux divergence.

The Eliassen-Palm flux divergence in the offline integration (Fig. 9a) during spring is almost two times larger than in the control integration (Fig. 9b). In this sense, the control integration shows a weak peak of $-6.9\,\mathrm{m\,s^{-1}\,day^{-1}}$ around day 294 (October 21st), while the offline integration has a peak of $-12\,\mathrm{m\,s^{-1}\,day^{-1}}$ around day 284. In the offline integration, there is also an

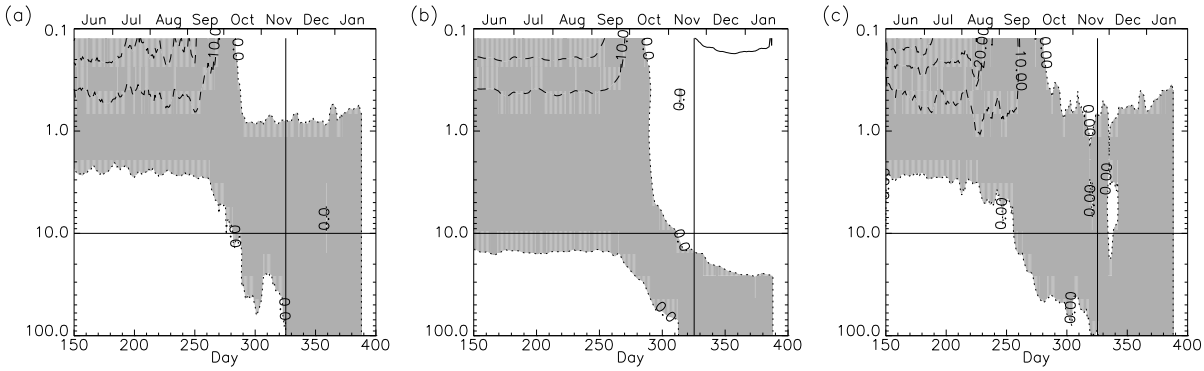

Figure 8. Zonal mean zonal gravity wave drag averaged between $50°\mathrm{S}$ and $80°\mathrm{S}$ as a function of time for (a) the offline integration, (b) the control integration and (c) the sequential integration. Contour interval is $5\,\mathrm{m\,s^{-1}\,day^{-1}}$. Negative values are shaded.

anticipation of the Eliassen-Palm flux divergence spring intensification. Hence, the rapid weakening of the winter jet can be attributed to the deceleration exerted by the larger amount of negative Eliassen-Palm flux divergence found in this integration during spring. The increase of Eliassen-Palm flux divergence with respect to the control integration appears as an indirect response to the changes in gravity wave drag. In this set of experiments, the effect on the circulation and on the index of refraction produced by the optimal parameters was a preconditioning of the middle atmosphere to focus the planetary wave events. This preconditioning is a characteristic of the sudden stratospheric warming events observed in the Northern hemisphere (McIntyre and Palmer 1983). Since the Southern hemisphere has a large deficit of planetary waves, in comparison to the Northern hemisphere, gravity waves play a more important role in the preconditioning for the stratospheric final warming. In the Northern hemisphere, planetary waves play a more active role in both the preconditioning and the stratospheric final warming itself, because of this the wind transition occurs first in the stratosphere and then in the mesosphere (Hardiman et al. 2011).

The middle atmosphere preconditioning can be seen as an indirect response to the optimized gravity wave drag. The different physical mechanisms that may lead to interactions between unresolved wave drag and resolved wave drag have been explained by Cohen et al. (2013). Scheffler and Pulido (2015) show that global perturbations to non-orographic gravity wave drag lead to changes in the mean circulation using the same model as in the current work. These changes in turn affect the refractive index of planetary waves and therefore, the Eliassen-Palm flux divergence. Similarly, Fig. 10a depicts that the use of optimal parameters from the offline method produces a stretching of the propagation waveguide in low latitudes with respect to the control integration (Fig. 10b). Furthermore, the use of optimal parameters produces a change of sign in the index of refraction in the lower mesosphere at latitudes polewards of $50°\mathrm{S}$. This behaviour persisted among the 7 years of this work. Since the change of sign is vertically steeper, planetary waves are forced to break in high latitudes, instead of being guided equatorwards as in the control integration (Fig. 10a). This is consistent with our hypothesis that the role of gravity wave drag is to produce a preconditioning so that planetary wave events, that propagate upon a reduced waveguide, induce the stratospheric final warming.

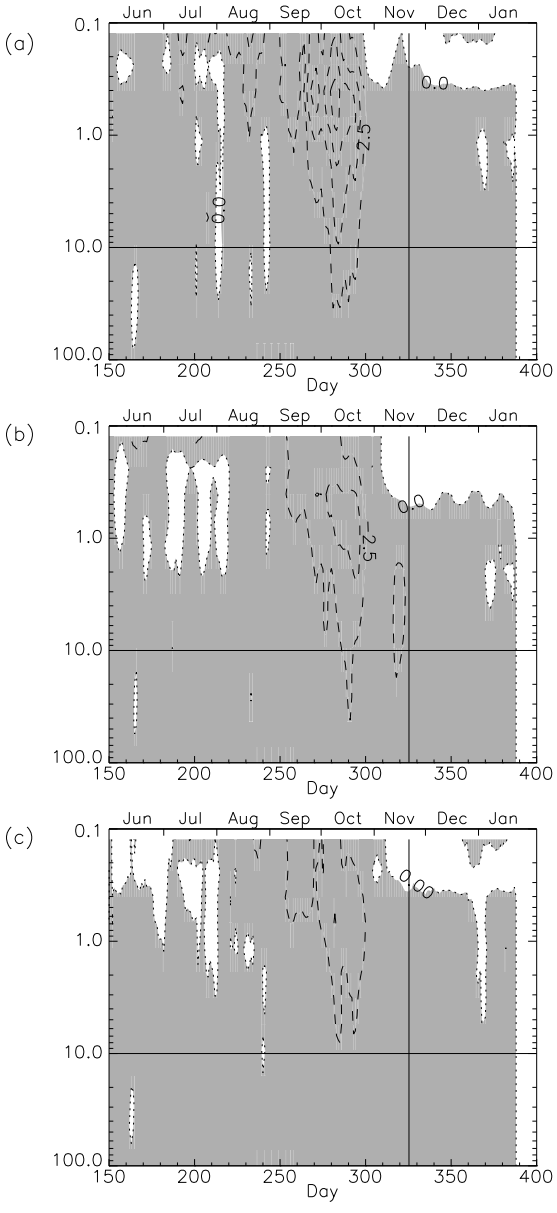

Figure 9. Eliassen-Palm flux divergence averaged between $50°\mathrm{S}$ and $80°\mathrm{S}$ as a function of time from (a) the offline integration, (b) the control integration and (c) the sequential integration. Contour intervals are $2.5\,\mathrm{m\,s^{-1}\,day^{-1}}$.

3.3. *Sequential parameter estimation experiments*

The optimal parameters estimated with the sequential method are also shown in Fig. 4 for a comparison with the ones estimated with the offline method. The annual cycle of the launched gravity wave momentum flux ($E*$) is similar to the one obtained with the offline method. There are differences in the magnitude of the parameter however. In the sequential method, E^* is larger than the one from the offline method by more than 50% during winter. The launched gravity wave momentum flux becomes weaker than its reference value after day 302 (October 29th). The peak and the subsequent decrease of launched gravity wave momentum flux occur around the same time in both offline and the sequential methods.

The relationship between λ^* and S^* parameters detected with the offline method is also found with the sequential method (thin lines in Fig. 4b). Specifically, they are anti-correlated up to day 260 (September 17th) and they are correlated between days 265 and 310 (September 22nd and November 6th respectively). During this period of time, the missing wave forcing estimated with ASDE is characterized by a strong eastward acceleration centre between $0.7\,\mathrm{hPa}$ and $0.24\,\mathrm{hPa}$ (Fig. 1b). The pronounced correlation between the parameters might be associated with the lack of wind shear during this period, which leads to a reduced drag deposition through filtering, leading the S^* parameter to play a more dominant role in the vertical structure of gravity wave drag. Parameter λ^* shows in general larger values than the ones from the offline method (this is, a larger characteristic phase speed c^*), implying that the spectral density will be larger for higher phase speeds. Therefore, there will be less wave momentum flux deposited in the lowest levels of the model.

The model integrations with optimal parameters estimated with the sequential method, are hereinafter referred to as *sequential integration*. As shown in Fig. 6c, the vertical and temporal structure of the zonal wind is largely improved during winter in the sequential integration with respect to the control and offline integrations, particularly in the higher stratosphere and above. The wind reversal at $60°\mathrm{S}$ at $10\,\mathrm{hPa}$ occurs on average at day 327 (November 27th), 5 days later than in MERRA and one day earlier than with the offline method. However, the vortex breakdown in the upper stratosphere and lower mesosphere occurs with a delay in the wind reversal at $0.1\,\mathrm{hPa}$ of 9 days with respect to the offline integration.

The resulting gravity wave drag for high latitudes from the sequential integration is shown in Fig. 8c. The vertical profiles obtained with both techniques are relatively similar, in comparison to the differences found with the gravity wave drag from the control integration. However, the sequential integration exhibits a larger deceleration during winter (days 150 to 244) in the higher stratosphere and above. This is in accordance with the estimated increase of launched momentum flux parameter. By the end of winter and the beginning of spring (days 230 to 290), the westward gravity wave drag above $0.4\,\mathrm{hPa}$ weakens earlier in the sequential integration, with differences in the gravity wave drag from the offline integration of up to $8.5\,\mathrm{m\,s^{-1}\,day^{-1}}$ at $0.1\,\mathrm{hPa}$ around day 273 (end of September). The differences in filtering of gravity waves in the experiments are partially driven by the different strengths of the winter jet core. On the other hand, the winter jet location is approximately the same in the three experiments, so it is discarded as a possible source of induced changes in gravity wave drag. The transition from westward forcing to eastward forcing in the top levels of the model takes place 4 days earlier than in the offline integration. Below $2\,\mathrm{hPa}$, the transition from eastward to westward forcing is anticipated by 20 days.

Figure 7a includes the zonal wind RMSE of the sequential integration. The sequential integration seems to outperform the offline integration in terms of RMSE during autumn and winter, due to the improvements in the representation of the jet intensity. Between days 290 and 315 (October 17th and November 11st), the offline integration shows a superior performance in terms of RMSE, related to the relative deficiencies of the sequential integration in the representation of the zonal wind transition above $1\,\mathrm{hPa}$. Temperature RMSE (Fig. 7b) is also improved when optimal parameters from the sequential method were used, except between days 290 and 320. The degraded performance during these days is due to a colder stratosphere in the sequential integration (not shown).

Both wind and temperature deficiencies between days 290 and 320 in the sequential integration are related to a lack of planetary wave drag, i.e. the model cannot represent properly the large-scale wave disturbances found between the days in the integration with offline optimal parameters (Fig. 6a). Indeed, the planetary wave drag under this configuration is overall weaker. As shown in Fig. 9c, the negative Eliassen-Palm flux divergence region during early spring —days 260 to 300— has smaller values than the other integrations, i.e. the peak of day 283 (October 10th) has a value of $-5.1\,\mathrm{m\,s^{-1}\,day^{-1}}$, which is even lower that the associated peak in the control integration, of $-6.25\,\mathrm{m\,s^{-1}\,day^{-1}}$. This effect is likely responsible for the delayed wind transition above $1\,\mathrm{hPa}$, with respect to the offline method.

The reduction in the planetary wave drag in the sequential integration can be associated with changes in the index of refraction, as a response to the optimized parameters in the gravity wave drag parameterization. Figure 10 shows the index of refraction for stationary waves and for wavenumber $s = 1$ averaged between days 240 and 280. The refraction index shows a widening of the waveguide towards the Equator for the sequential integration (Fig. 10c), respect to the offline integration (Fig. 10a). Additionally, the propagation threshold $n^2 < 0$ in high latitudes is slightly displaced towards the Equator in the sequential integration. Overall, the index of refraction in the sequential integration in mid and high latitudes shows a broader horizontal gradient that enforces propagation towards the Equator instead of wave breaking. A similar effect was found for wavenumber $s = 2$ (not shown). This suggests that planetary wave breaking in high latitudes in the sequential method is effectively being reduced since the middle atmosphere was not preconditioned (by the effects of gravity wave drag).

The sequential method estimates optimal parameters that try to represent not only missing gravity wave drag but also unrepresented Eliassen-Palm flux divergence and some of the gravity-wave planetary-wave interactions. A similar result was reported by Ruiz and Pulido (2015) which found that the estimated convective parameters diminish not only the error associated with convective processes but also error sources associated with boundary layer processes. Although

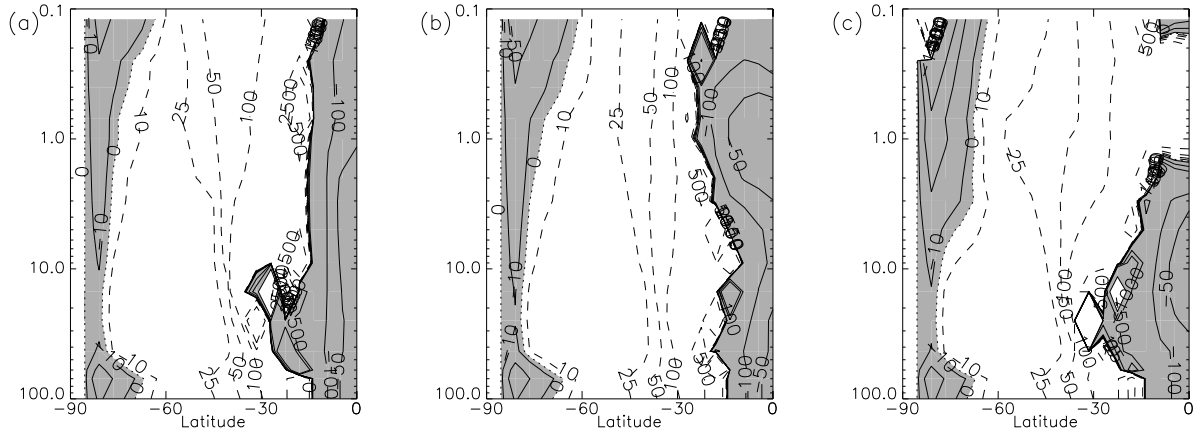

Figure 10. Quasi-geostrophic index of refraction (non-dimensionalized) n^2 for wavenumber $s = 1$ averaged between days 240 and 280. (a) Offline integration, (b) control integration, (c) sequential integration. A logarithmic scale is used and negative values are shaded.

this may reduce the model error in some situation, it is likely to result in a degradation of the process represented by the parameterization.

4. Conclusions

In this work, we examine the impact of estimating optimal parameters for a non-orographic gravity wave drag parameterization on the model integration during final stratospheric warmings. The missing forcing in a middle atmosphere model is estimated using a 4d-Var data assimilation technique and reanalysis data from MERRA. The estimated missing forcing at high latitudes exhibits a strong deceleration during winter with peaks of up to $-36\,\mathrm{m\,s^{-1}\,day^{-1}}$. This deceleration (westward) centre is followed by a change to eastward gravity wave drag around mid September. The Eliassen-Palm flux divergence shows a large sink of planetary wave momentum flux during the zonal wind transition, which is also reproduced accurately by ASDE. The ability to estimate realistically both resolved and unresolved wave drag with a data assimilation technique has a large potential in terms of development, improvement or tuning of gravity wave drag parameterizations.

The two proposed parameter estimation methods show promising results in terms of representing the final stratospheric warming more closely to observations. The integrations with parameters from the offline method shows a delay in the final warming date of 6 days at $10\,\mathrm{hPa}$ at $60°\mathrm{S}$. In this integration, the anticipation of the wind reversal during spring is achieved through an improvement of the planetary wave breaking, which is closer to Eliassen-Palm flux divergence from MERRA. This improvement is an indirect response to a preconditioning of the mean circulation via changes introduced by the gravity wave drag. The mean flow circulation during winter, however, is not improved above $10\,\mathrm{hPa}$.

When using optimal parameters estimated through the sequential method, the final stratospheric warming date is similar to the offline method (the delay is reduced by one day). The overestimation of zonal wind intensity during winter above $1\,\mathrm{hPa}$ given by the offline and the control integration is largely corrected. In spite of these improvements, the integration with parameters from the sequential method shows an important lack of planetary wave drag with respect to observations. This introduces a delay in the zonal wind reversal above $1\,\mathrm{hPa}$ at high latitudes of up to 9 days with respect to the integration with parameters from the offline method.

The optimal parameters found with both techniques follow a relatively similar temporal regime. The temporal and latitudinal variability patterns suggests that a parameterization of gravity waves sources (as in Bushell et al. 2015) is necessary and could lead to improved results with respect to fixed sources. Additionally, the estimated gravity wave parameters could be compared with tropospheric data to identify which gravity wave sources play the most decisive role in the seasonal cycle of gravity wave drag. Filtering in the troposphere may also play a role in the obtained seasonal cycle (Manzini and McFarlane 1998). Regrettably, the middle atmosphere model used in this work does not allow us to optimize the launching height of the waves in the parameterization since it does not represent the troposphere.

While the aim of this work was not to find which of the proposed methods is better, the differences found in planetary wave drag during spring with each method emphasize the importance of properly reproducing the interactions between gravity wave drag and planetary wave propagation. When using parameters from the offline method, the breaking of planetary waves plays an active role in the wind reversal and the mean flow is preconditioned to enhance planetary wave activity. The dynamical mechanism that avoids the preconditioning for planetary wave breaking in the experiments with the sequential method is not completely understood. A possible hypothesis is that sequential methods attempts to fix all systematic missing momentum sources in the model, including an incorrect planetary wave drag representation, through a direct optimization of the gravity wave drag parameterization. In this sense, the correct transition found in the sequential method is a consequence of the gravity wave parameterization through the daily corrections of forcing terms. These corrections may suppress other potential contributors involved in the winter-summer transition that require a certain amount of time to ramp up, i.e. changes in the planetary wave breaking induced by modulation of the planetary waveguide. In more general terms, the sequential method is able to give the correct

answer but based on incorrect causes. On the other hand, all the missing momentum sources in the offline method are continuously fixed by the assimilation system so that the optimal gravity wave parameters are estimated for a circulation and a planetary wave distribution that is close to the one found in observations (MERRA reanalysis). This method appears to account better for the subtle feedback mechanisms between unresolved gravity wave drag and planetary waves.

Acknowledgement

This work was partially funded by an Agencia Nacional de Promoción Científica y Tecnológica grant PICT2015-2368 and a CONICET grant PIP 112-20120100414CO. Simulations were performed using computational facilities at CECONEA (UNNE).

References

Alexander MJ, Geller M, McLandress C, Polavarapu S, and co-authors. 2010. Recent developments in gravity wave effects in climate models and the global distribution of gravity wave momentum flux from observations and models. *Quart. J. Roy. Meteor. Soc.*, **136**, 1103–1124.

Alexander MJ, Rosenlof KH. 1996. Nonstationary gravity wave forcing of the stratospheric zonal mean wind. *J. Geoph. Res.*, **101**, 23465–23474.

Anderson J. 2001. An Ensemble Adjustment Kalman Filter for Data Assimilation. *Mon. Wea. Rev.*, **129**, 2884–2903.

Annan JD, Hargreaves JC, Edwards NR, Marsh R. 2005. Parameter estimation in an intermediate complexity earth system model using an ensemble Kalman filter. *Ocean modelling*, **8**, 135–154.

Austin J, Shindell D, Beagley SR, Brühl C, Dameris M, Manzini E, and Coauthors. 2003. Uncertainties and assessments of chemistry climate models of the stratosphere. *Atmos. Chem. Phys.*, **3**, 1–27.

Bloom SC, Takacs LL, Da Silva AM, Ledvina D. 1996. Data assimilation using incremental analysis updates. *Mon. Wea. Rev.*, **124**, 1256–1271.

Bushell, AC, Jackson DR, Butchart N, Hardiman SC, Hinton TJ, Osprey SM, Gray LJ. 2010. Sensitivity of GCM tropical middle atmosphere variability and climate to ozone and parameterized gravity wave changes. *J. Geophys. Res.*, 115(D15).

Bushell, A. C., Butchart, N., Derbyshire, S. H., Jackson, D. R., Shutts, G. J., Vosper, S. B., Webster, S. 2015. Parameterized gravity wave momentum fluxes from sources related to convection and large-scale precipitation processes in a global atmosphere model. *J. Atmos. Sci.*, **72**, 4349–4371.

Charbonneau P. 2002. An introduction to genetic algorithms for numerical optimization. Technical Note TN-450+IA. NCAR: Boulder, MA.

Cohen NY, Gerber EP, Bühler, O. 2013. Compensation between resolved and unresolved wave driving in the stratosphere: Implications for downward control. *J. Atmos. Sci.*, **70**, 3780–3798.

Cohen, N. Y., Gerber, E. P., Bühler O., 2014: What Drives the Brewer-Dobson Circulation?. *J. Atmos. Sci.*, **71**, 3837–3855.

de la Cámara, A., Lott, F., and Hertzog, A. 2014. Intermittency in a stochastic parameterization of nonorographic gravity waves. *J. Geophys. Res.*, 119(21).

de la Camara A, Lott F, Jewtoukoff V, Plougonven R, Hertzog A. 2016. On the gravity wave forcing during the southern stratospheric final warming in LMDz. *J. Atmos. Sci.*, **73**, 3213–3226.

Eyring V, Butchart N, Waugh DW, Akiyoshi H, Austin J, and Coauthors. 2006. Assessment of temperature, trace species, and ozone in chemistry climate model simulations of the recent past. *J. Geophys. Res.*, **111**, D22308.

Goldberg DE, Holland JH. 1988. Genetic algorithms and machine learning. *Machine learning*, **3**, 95-99.

Hardiman, S. C., Butchart, N., Charlton-Perez, A. J., Shaw, T. A., Akiyoshi, H., Baumgaertner, A., and co-authors. 2011. Improved predictability of the troposphere using stratospheric final warmings. *J. Geophys. Res.*, 116(D18).

Hines CO. 1997. Doppler-spread parameterization of gravity-wave momentum deposition in the middle atmosphere. Part 1: Basic formulation. *J. Atmos. Sol.-Terr. Phys.*, **59**, 371-386.

Lindzen RS. 1981. Turbulence and stress owing to gravity wave and tidal breakdown. *J. Geophys. Res.*, **86**, 9707-9714.

Long DJ, Jackson DR, Thuburn J. 2014. Offline estimates and tuning of mesospheric gravity-wave forcing using Met Office analyses. *Q. J. R. Meteorol. Soc.*, **140**, 1025-1038.

Lott, F., Guez, L. 2013. A stochastic parameterization of the gravity waves due to convection and its impact on the equatorial stratosphere. *J. Geophys. Res.*, 118, 8897-8909.

Manzini E, McFarlane NA. 1998. The effect of varying the source spectrum of a gravity wave parameterization in a middle atmosphere general circulation model, *J. Geophys. Res.*, **103**, 31523–31539.

McIntyre M, Palmer T. 1983. Breaking planetary waves in the stratosphere. *Nature*, **305**, 593–600.

McLandress C, McFarlane NA. 1993. Interactions between orographic gravity wave drag and forced stationary planetary waves in the winter Northern Hemisphere middle atmosphere. *J. Atmos. Sci.*, **50**(13), 1966-1990.

McLandress C, Shepherd TG, Polavarapu S, Beagley SR. 2012. Is missing orographic gravity wave drag near 60° S the cause of the stratospheric zonal wind biases in chemistry climate models?. *J. Atmos. Sci.*, **69**, 802-818.

Orr A, Bechtold P, Scinocca J, Ern M, Janiskova M. 2010. Improved middle atmosphere climate and forecasts in the ECMWF model through a nonorographic gravity wave drag parameterization. *J. Climate*, **23**, 5905–5926.

Pulido M, Thuburn J. 2005. Gravity wave drag estimation from global analyses using variational data assimilation principles. I: Theory and implementation. *Q. J. R. Meteorol. Soc.*, **131**, 1821–1840.

Pulido M, Thuburn J. 2006. Gravity wave drag estimation from global analyses using variational data assimilation principles. II: Case study. *Q. J. R. Meteorol. Soc.*, **132**, 1527–1543.

Pulido M, Thuburn J. 2008. The seasonal cycle of gravity wave drag in the middle atmosphere. *J. Climate*, **21**, 4664–4679.

Pulido M, Polavarapu S, Shepherd TG, Thuburn J. 2012. Estimation of optimal gravity wave parameters for climate models using data assimilation. *Quart. J. R. Meteorol. Soc.*, **138**, 298–309.

Pulido M. 2014. A simple technique to infer the missing gravity wave drag in the middle atmosphere using a general circulation model: Potential vorticity budget. *J. Atmos. Sci.*, **71**, 683–696.

Randall, DA, Wielicki BA. 1997. Measurements, models, and hypotheses in the atmospheric sciences. *Bulletin of the American Meteorological Society*, **78**, 399–406.

Rienecker MM, Suarez MJ, Gelaro R, Todling R, Bacmeister J, Liu E, and Coauthors. 2011. MERRA: NASA's Modern-Era Retrospective Analysis for Research and Applications., *J. Climate*, **24**, 3624-3648.

Ruiz J., M. Pulido and Miyoshi T. 2013. Estimating parameters with ensemble-based data assimilation. A review. *J. Meteorol. Soc. Japan*. **91**, 79–99.

Ruiz J. and Pulido M. 2015. Parameter estimation using ensemble based data assimilation in the presence of model error. *Mon. Wea. Rev.*, **143**, 1568–1582.

Scheffler G, and Pulido M. 2015. Compensation between resolved and unresolved wave drag in the stratospheric final warmings of the Southern hemisphere. *J. Atmos. Sci.*, **72**, 4393–4411.

Scinocca JF. 2003. An accurate spectral non orographic gravity wave drag parameterization for general circulation models. *J. Atmos. Sci.*, **60**, 667–682.

Scinocca JF, McFarlane NA, Lazare M, Li J, Plummer D. 2008. Technical Note: The CCCma third generation AGCM and its extension into the middle atmosphere. *Atmos. Chem. Phys.*, **8**, 7055-7074.

Shepherd TG, Shaw TA. 2004. The angular momentum constraint on climate sensitivity and downward influence in the middle atmosphere. *J. Atmos. Sci.*, **61**, 2899–2908.

Thuburn J. 1997. A PV based shallow water model on a hexagonal icosahedral grid. *Mon. Wea. Rev.*, **125**, 2328–2347.

Warner CD, McIntyre ME. 1996. On the propagation and dissipation of gravity wave spectra through a realistic middle atmosphere. *J. Atmos. Sci.*, **53**, 3213–3235.